17th World Conference on Earthquake Engineering, 17WCEE
Sendai, Japan - September 27th to October 2nd, 2021

Shaking Table Test of a Base-isolated Building Model Considering Seismic Pounding of a Retaining Wall

T. Chuman[(1)], K. Fujii[(2)]

[(1)] *Graduate Student, Chiba Institute of Technology, s16b1109uj@s.chibakoudai.jp*
[(2)] *Professor, Dr. Eng., Chiba Institute Technology, kenji.fujii@it-chiba.ac.jp*
…

Abstract

Seismic isolation is one of the most attractive techniques for earthquake protection in buildings. Unlike traditional techniques used in constructing earthquake-resistant buildings, this technique can reduce floor accelerations appreciably during a strong earthquake. Although the base-isolation technique is widely applied to many new buildings in earthquake-prone countries, these buildings require sufficient clearance for horizontal movement during large earthquakes. In the case of an excessively large seismic excitation, some base-isolated buildings with insufficient clearance may strike the surrounding retaining wall. Pounding by base-isolated buildings may severely damage the superstructure in the event of excessively large acceleration responses. Although there have been analytical and experimental studies on this issue, to the best of the authors' knowledge, few studies have focused on the energy response of such base-isolated buildings considering seismic pounding.

The present paper experimentally investigates the effect of the seismic pounding behavior of a base-isolated building on a retaining wall. The criterion for the seismic pounding of a base-isolated building is then discussed in terms of the maximum momentary energy input.

The test models used in this study are three-story base-isolated structural models. The base-isolation layer of the test model comprises four caster wheels and coil springs, allowing the simulation of horizontal movement. The stiffness of coil springs is determined considering the ratio of the isolated period and the natural period of the fixed-base model. The parameters of the shaking table test are (i) the size of the clearance and (ii) the stiffness of the superstructure. Four recorded horizontal ground motions are used in the test.

The following findings are taken from the test results.

(1) In the case of a flexible superstructure, the increase in acceleration due to pounding is limited to the lowest floor. In contrast, the acceleration increases appreciably on all floors in case of a stiff superstructure.

(2) The story shear in the superstructure of the base-isolated model may be larger than that in the superstructure of the fixed-based model.

(3) The equivalent velocity of the maximum momentary input energy, calculated from test results, is close to the elastic input energy spectra. The difference in the maximum momentary input energy due to the clearance size is negligible.

The criterion for the seismic pounding of a base-isolated building is then discussed in terms of the energy balance per half cycle of the response. The capacity of energy absorption at the base-isolation layer, $\Delta E_{\mu BI}$, is calculated assuming the maximum deformation of the isolation layer equals the size of the clearance. The ratio of ΔE_{BI} to the maximum momentary input energy, $\Delta E_{\max}$, is then calculated. The test results show that the ratio ($\Delta E_{\mu BI}/\Delta E_{\max}$) is a potential possible index with which to judge the possibility of seismic pounding. The ratio ($\Delta E_{\mu BI}$ /$\Delta E_{\max}$) should be larger than unity to avoid seismic pounding.

Keywords: Base Isolation, Seismic Pounding, Shaking Table Test, Momentary Input Energy

1. Introduction

A seismically isolated system is an attractive structural system because of its ability to reduce floor acceleration [1]. The base isolation technique has thus been widely applied to new buildings and the seismic upgrading of existing buildings in recent years. A base-isolated building requires sufficient clearance for horizontal movement during large earthquakes. However, there are concerns about the effects of long-period long-duration ground motion on base-isolated buildings [2]. In the case of an excessively large seismic excitation, some base-isolated buildings with insufficient clearance may strike a surrounding retaining wall, and pounding by a base-isolated building may severely damage the superstructure in the event of excessively large acceleration responses. Although there have been analytical [e.g., 3–6] and experimental [7] studies, to the best of the authors' knowledge, few studies have focused on the energy response of base-isolated buildings considering seismic pounding.

The present paper experimentally investigates the effect of the seismic pounding behavior of a base-isolated building on a retaining wall. A criterion for the seismic pounding of a base-isolated building is then discussed in terms of the maximum momentary energy input proposed by Hori and Inoue [8].

2. Outline of the experiment

2.1 Building model

Figure 1 shows the three-story base-isolated model used in the present study. In this study, two base-isolated models are adopted for consideration of different values of horizontal stiffness of the superstructure. The columns in the superstructure are aluminum plates, each having a height of 260 mm and width of 80 mm. The thickness of columns in Model-1 (a flexible superstructure) is 1.0 mm while that of columns in Model-2 (a stiff superstructure) is 1.5 mm. The level-0 floor is a single plate having thickness of 15 mm while the upper floors each have two 10-mm-thick plates. The base-isolation layer in each of the models comprises four caster wheels and eight coil springs, allowing simulation of horizontal movement. The coefficient of rolling friction of a caster wheel is 0.08 while the stiffness of a coil spring is 14 N/m.

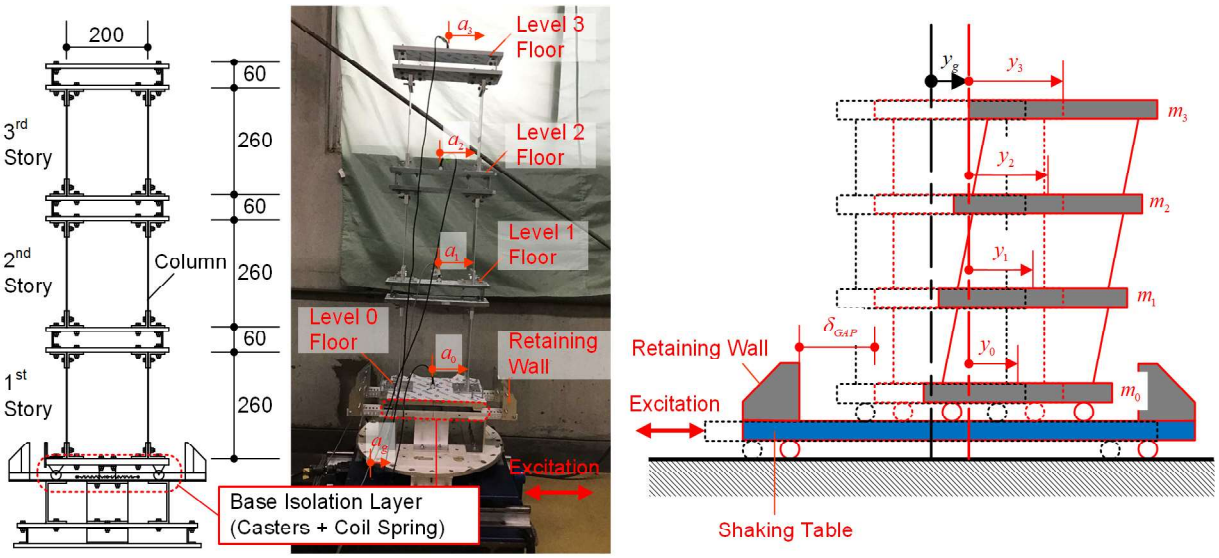

(a) Test specimen (b) Model of the test specimem

Figure – 1 Base-isolated building model

Table 1 gives the mass of each floor, m_j (j = 0 to 3), in the models.

Table – 1 Floor masses in the models

	Model-1	Model-2
Level 3 Floor: m_3 (kg)	2.075	2.100
Levels 1 and 2 Floor: m_1, m_2 (kg)	2.450	2.500
Level 0 Floor: m_0 (kg)	2.859	2.890

The natural period of the superstructure is obtained in a sweep excitation test. In the test, horizontal movement of the base-isolation layer is restricted using vises. The natural period of the first mode of the superstructure, T_{1FIX}, is 0.607 s (Model-1) and 0.329 s (Model-2). The isolated period without considering the coefficient of rolling friction, T_f, is 1.938 s (Model-1) and 1.899 s (Model-2). Therefore, the ratio T_f/T_{1FIX} is 3.19 for Model-1 and 5.77 for Model-2.

In this test, retaining walls are placed either side of the base-isolated model, as shown in Fig. 1(a). These walls are also made of aluminum alloy and are stiff. The clearance, δ_{gap}, is set to 15, 25, 35, and 45 mm, and to 0 mm for the fixed-base isolated model.

2.2 Input seismic wave and measurement plan

A shaking table test is performed for four adjusted input seismic waves. The target peak acceleration and time interval are scaled to adjust the maximum movement of the shaking table to within the allowable limit. Specifically, the target peak accelerations of three waves, namely El Centro 1940NS (ELC), Hachinohe 1968NS (HAC), and JMA Kobe (JKB), are scaled to 40% of gravitational acceleration, and the time intervals are scaled by 50%. Meanwhile, the time interval of Sylmar 1994NS (SYL) is scaled by 59%. Figure 2 shows spectra of the equivalent velocity of the cumulative input energy and the maximum momentary input energy [8].

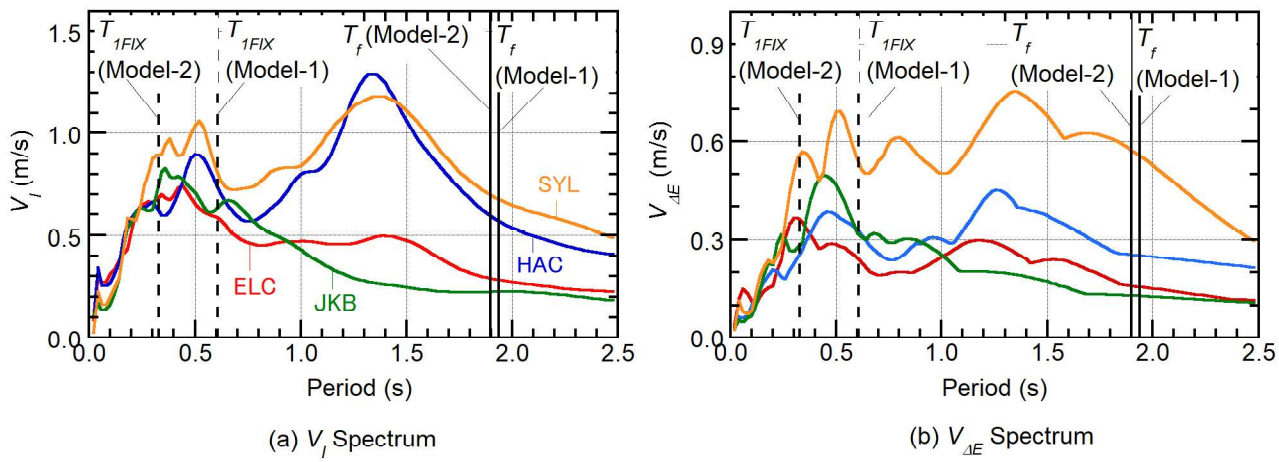

Figure – 2 V_I and $V_{\Delta E}$ spectra

The absolute accelerations of each floor $a_j(t)$ and the shaking table $a_g(t)$ are measured by placing one accelerometer on each floor. The relative displacement of each floor $y_j(t)$, shown in Fig. 1(b), is calculated according to

$$y_j(t) = \int_0^t v_j(t)dt, v_j(t) = \int_0^t \{a_j(t) - a_g(t)\}dt. \quad (1)$$

In the calculation of Eq. (1), the components of the relative velocity $v_j(t)$ having a frequency less than 0.6 Hz are removed to avoid cumulative error in the integration in Eq. (1). The resultant of the horizontal inertial force above each story, $Q_j(t)$, is calculated as

$$Q_j(t) = -\sum_{k=j}^{3} m_k a_k(t). \quad (2)$$

In the superstructure $(j \geq 1)$, $Q_j(t)$ is the story shear. However, in the base-isolation layer $(j = 0)$, $Q_0(t)$ obtained from Eq. (2) is the resultant of the story shear in the base-isolation layer and reaction force of the retaining wall.

3. Test results

3.1 Time history responses

Figure 3 shows the time history of the acceleration at level 0 and the resultant of story shear above the isolation layer, $a_0(t)$ and $Q_0(t)$ respectively, for a case in which pounding occurred (Model-1, δ_{gap} = 15 mm, input wave: HAC). Sharp spikes in $a_0(t)$ are evident after 16 seconds. A sharp spike in the acceleration response is considered here as a "pounding". Sharp spikes in $Q_0(t)$ also show that "pounding" occurs.

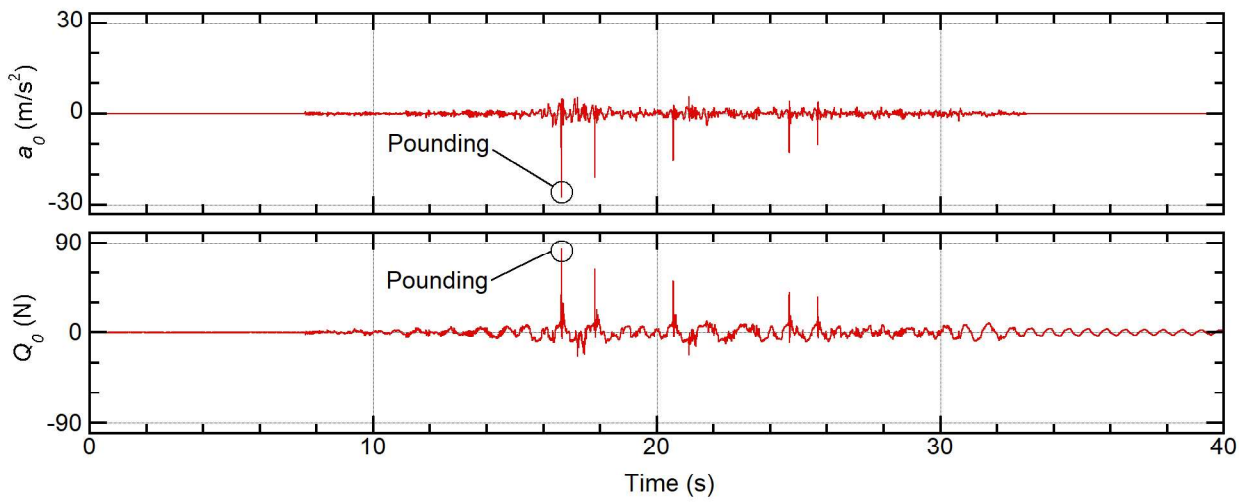

Figure – 3 Time history of acceleration at level 0 and the resultant above the isolation layer

3.2 Peak acceleration of each floor

Figure 4 compares the peak acceleration at each floor obtained from the test results for different clearances. Figure 4(a1) and (a2) shows the results for HAC while Fig. 4(b1) and (b2) shows the results for SYL. As shown in Fig. 4(a1), the response acceleration at the floor level 0 of Model-1 increases appreciably as δ_{gap} decreases. However, the increase in acceleration of upper floors is negligible. In contrast, the acceleration of all floors of Model-2 is appreciably higher when δ_{gap} is 15 mm, as shown in Fig. 4(a2).

In Fig. 4(b1), the peak acceleration is largest on all floors when δ_{gap} is 35 mm in Model-1. In Fig. 4(b2), the peak acceleration at floor level 1 is largest when δ_{gap} is 25 mm in Model-2.

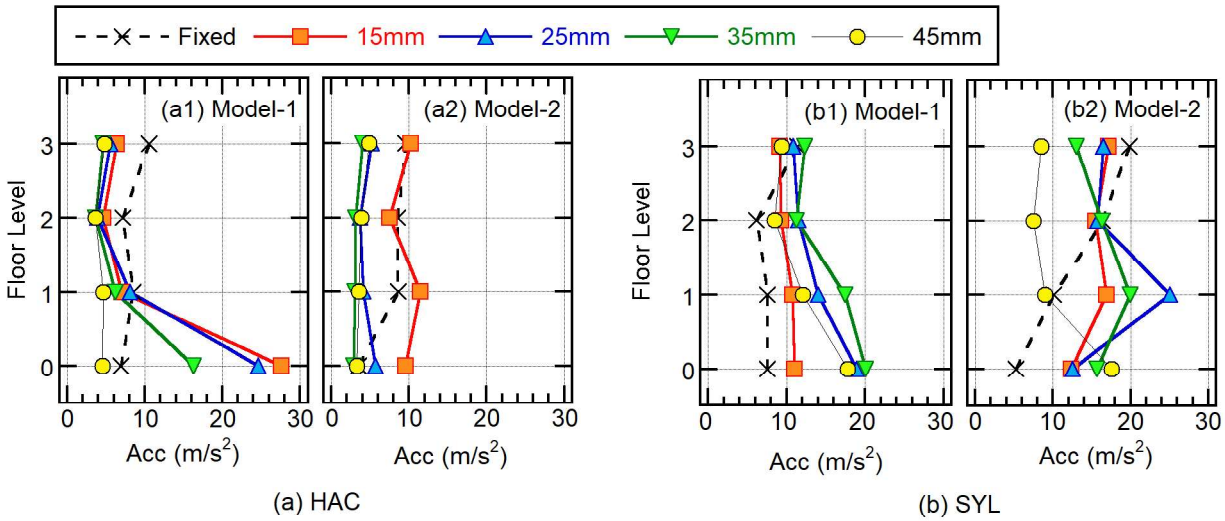

Figure – 4 Peak floor acceleration

3.3 Maximum story shear in the superstructure

Figure 5 compares the maximum story shear, $Q_{j\max}$, in the superstructure obtained from the test results for different clearances. Figure 5(a1) and (a2) shows the results for HAC while Fig. 5(b1) and (b2) shows the results for SYL.

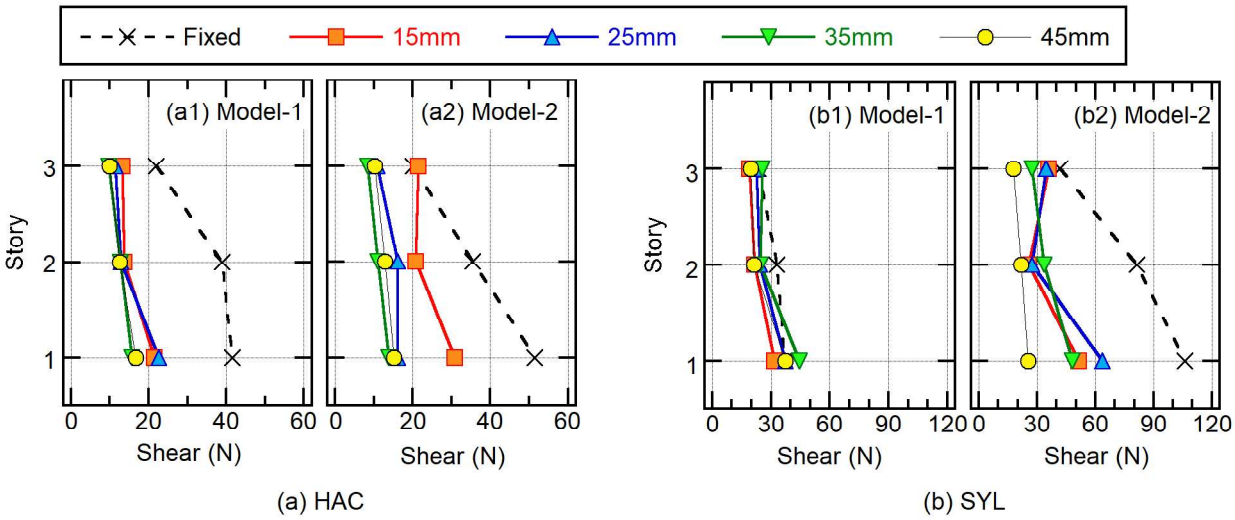

Figure 5 – Maximum story shear in the superstructure

In Fig. 5(a1), the effect of the clearance size on the maximum story shear is limited in the case of Model-1. However, in the case of Model-2 shown in Fig. 5(a2), the effect of the clearance size on the

maximum story shear is notable; i.e., the story shear increases as the clearance δ_{gap} decreases. In the case that δ_{gap} is 15 mm, the maximum story shear on the third story, $Q_{3\max}$, is larger than that for the fixed-base fixed model.

In Fig. 5(b1), the maximum story shear on the first story, $Q_{1\max}$, is largest when δ_{gap} is 35 mm. In Fig. 5(b2), the maximum story shear on the first story, $Q_{1\max}$, is largest when δ_{gap} is 25 mm.

In conclusion, the story shear in the superstructure of the base-isolated model may be larger than that for the fixed-base model owing to pounding. However, the clearance that produces the largest story shear in the superstructure depends on the characteristics of the ground acceleration and the dynamic properties of the base-isolated structure.

4. Evaluation of maximum momentary input energy

This section evaluates the maximum momentary input energy to investigate a criterion for the seismic pounding of a base-isolated building according to the energy balance per half cycle of the response.

4.1 Definitions of the per half cycle of the response and momentary input energy

The present paper considers the energy balance per half cycle of the response, following the work of Hori and Inoue [8]. The velocity of the center of gravity, $v(t)$, is calculated as

$$v(t) = \sum_{j=0}^{3} m_j v_j(t) / \sum_{i=0}^{3} m_i \,. \tag{3}$$

The cumulative input energy from the beginning to time t, $E_I(t)$, and the kinetic energy at time t, $E_V(t)$, are defined as

$$E_I(t) = -\int_0^t \sum_{j=0}^{3} m_j a_g(t) v_j(t) dt \,, \tag{4}$$

$$E_V(t) = \frac{1}{2} \sum_{j=0}^{3} m_j \{v_j(t)\}^2 \,. \tag{5}$$

Figure 6 shows the time history of $v(t)$, $E_I(t)$, and $E_V(t)$. In this study, the times of the beginning and end of the half cycle, t_1 and t_2 respectively, correspond to $v(t)=0$, as shown in Fig. 6(a). Figure 6(b) shows that the kinetic energy $E_V(t)$ is at a local minimum when $t=t_1$ and $t=t_2$. Following the definition of Hori and Inoue [8], the momentary input energy ΔE from $t=t_1$ to $t=t_2$ is defined as

$$\Delta E = E_I(t_2) - E_I(t_1) = -\int_{t_1}^{t_2} \sum_{j=0}^{3} m_j a_g(t) v_j(t) dt \,. \tag{6}$$

The maximum momentary input energy, $\Delta E_{\max}$, is defined as the maximum value of ΔE over the course of the seismic event. The equivalent velocity of the maximum momentary input energy is defined as

$$V_{\Delta E} = \sqrt{\frac{2\Delta E_{\max}}{M}}, M = \sum_{j=0}^{3} m_j \,. \tag{7}$$

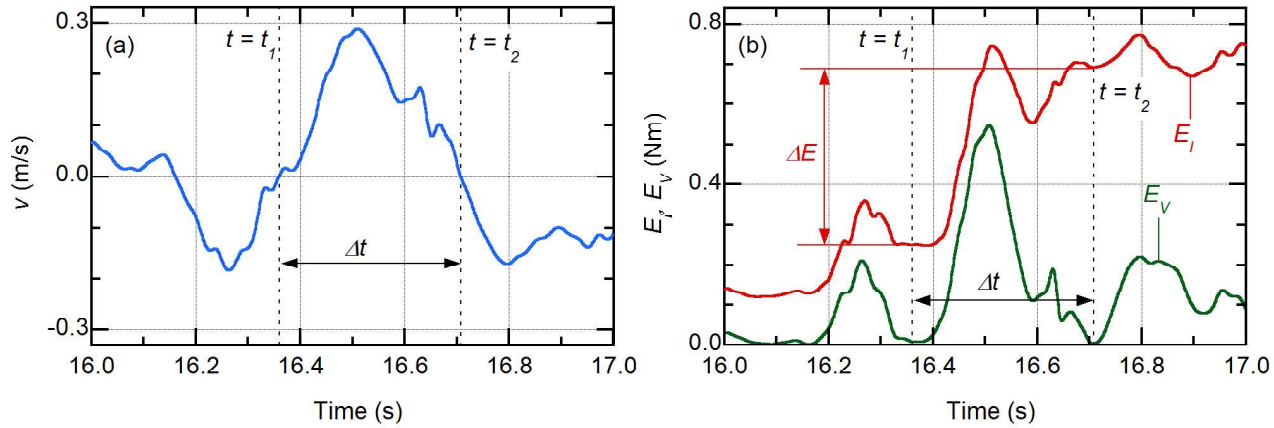

Figure 6 – Definition of the momentary energy input: (a) time history of $v(t)$ and (b) time history of $E_I(t)$ and $E_V(t)$.

4.2 Comparison of the maximum momentary input energy

Figures 7 and 8 show the time history responses of the momentary input energy in the case of Model-1 for HAC. The case that clearance δ_{gap} = 15 mm is shown in Fig. 7 while the case that δ_{gap} = 45 mm is shown in Fig. 8.

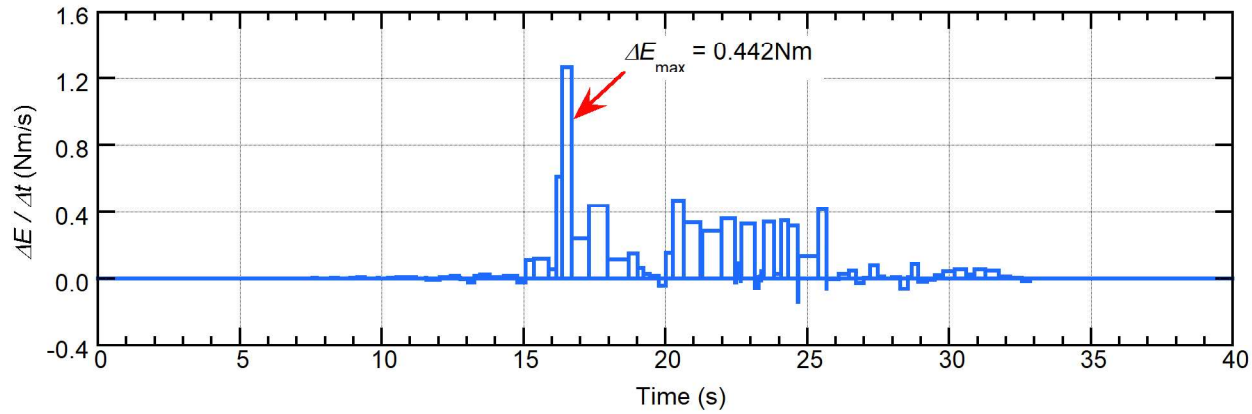

Figure – 7 Time history response of the momentary input energy (clearance of 15 mm)

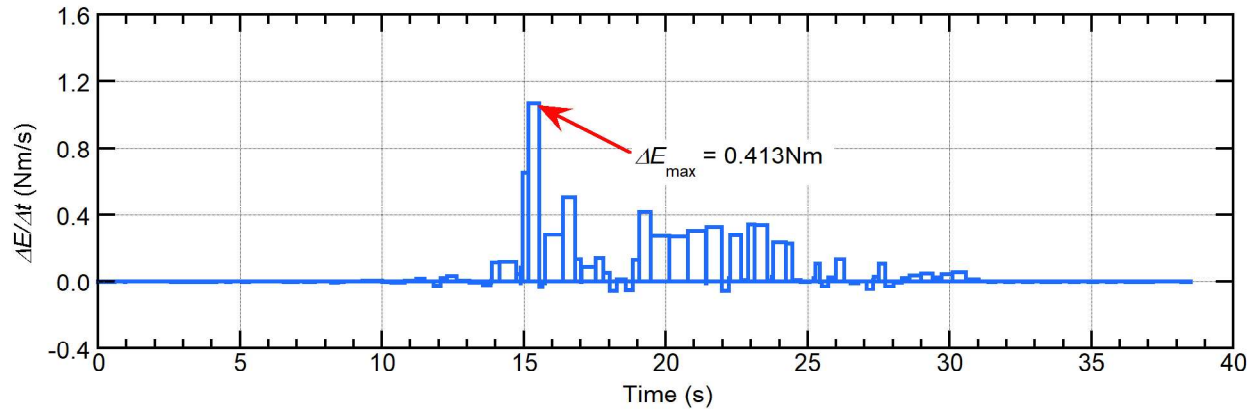

Figure – 8 Time history response of the momentary input energy (clearance of 45 mm)

In the case that δ_{gap} = 15 mm shown in Fig. 7, pounding occurs after approximately 16 seconds, when ΔE reaches a maximum value. In case that δ_{gap} = 45 mm shown in Fig. 8, there is no collision. The maximum momentary input energy when δ_{gap} = 15 mm is 0.442 Nm, while that when δ_{gap} = 45 mm is 0.413 Nm. The difference in $\Delta E_{\max}$ due to pounding is therefore limited. In addition, the time histories of the momentary energy input are similar for the two values of δ_{gap} .

Figure 9 shows the equivalent velocity of the maximum momentary input energy, $V_{\Delta E}$, compared by clearance δ_{gap} . Figure 9(a) shows that the value of $V_{\Delta E}$ is stable in the case of HAC; i.e., differences due to the size of the clearance and stiffness of the superstructure are negligible. By contrast, in the case of SYL shown in Fig. 9(b), $V_{\Delta E}$ decreases slightly as the clearance δ_{gap} increases. The difference in $V_{\Delta E}$ due to the difference in superstructure is small.

Figure 10 compares the equivalent velocity $V_{\Delta E}$ obtained from the test results shown in Fig. 9 and the elastic $V_{\Delta E}$ spectrum (Fig. 2(b)). In this figure, the effective period of the test results T' is assumed to be twice the time of the half cycle of the response when the energy input is a maximum.

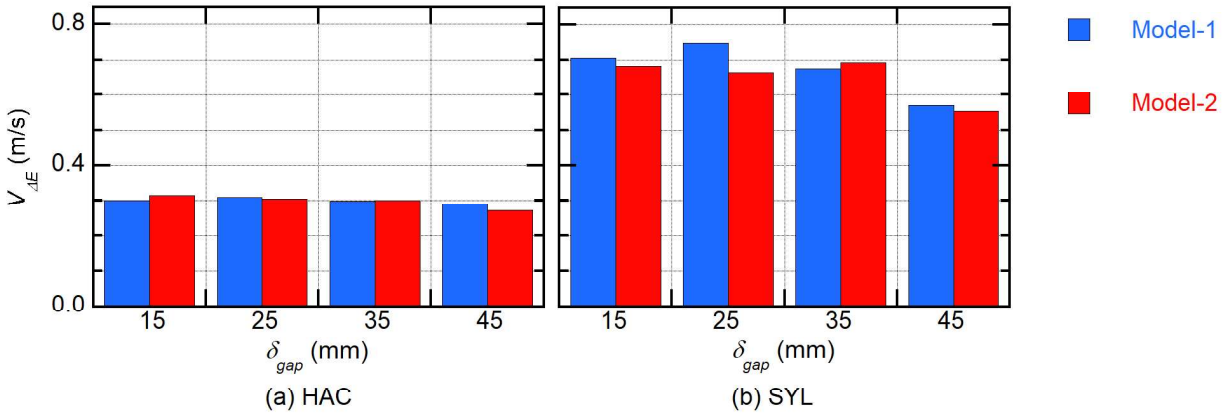

Figure – 9 Comparison of the maximum momentary input energy

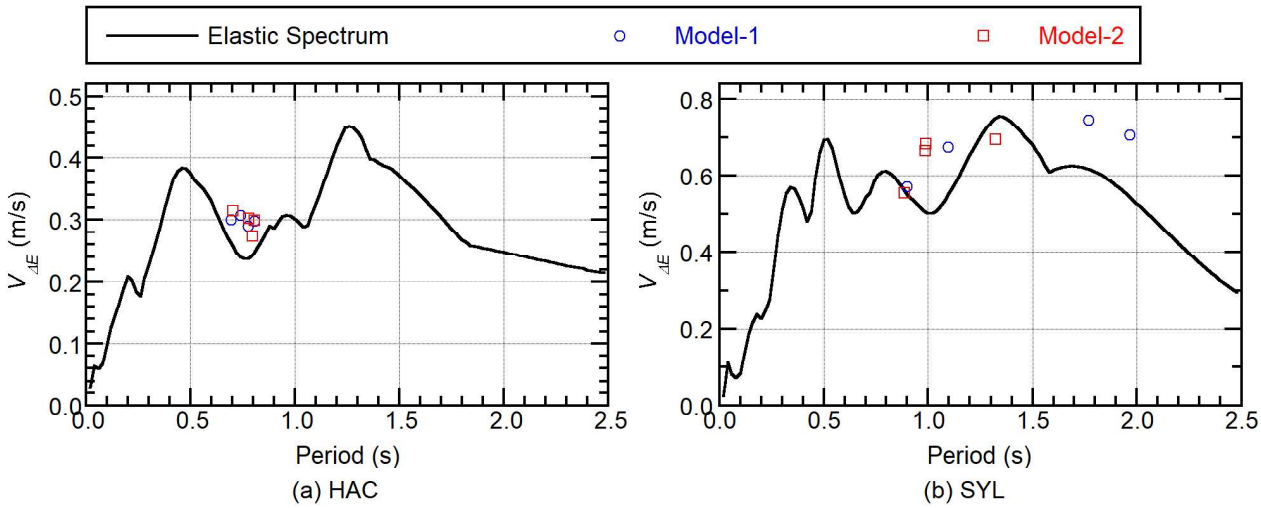

Figure – 10 Comparison of the equivalent velocity obtained from the test results and the elastic spectrum

In Fig. 10, the plots of the test results are close to the elastic $V_{\Delta E}$ spectra. Therefore, the maximum momentary input energy $\Delta E_{\max}$ of the base-isolated building may be evaluated from the elastic $V_{\Delta E}$ spectrum, if the effective period can be properly evaluated.

5. Criterion for the seismic pounding of a base-isolated building

This section discusses a criterion for the seismic pounding of a base-isolated building in terms of the energy balance per half cycle of the response.

5.1 Evaluation of the capacity of energy absorption at the base-isolation layer

Figure 11 shows the modeling of absorbable energy at the base-isolation layer per half cycle of the response. Here, the flexible element shown in Fig. 11(b) represents the elastic behavior of coil springs (i.e., horizontal stiffness of coil springs, k_{0f}) while the rigid-plastic element shown in Fig. 11 (c) represents the rigid-plastic behavior of caster wheels (i.e., rolling friction force of caster wheels, ${}_sQ_{0y}$). The capacity of energy absorption at the base-isolation layer, $\Delta E_{\mu BI}$, is calculated as the sum of the energy absorption of the flexible element, $\Delta_f E_{\mu BI}$, and rigid-plastic element, $\Delta_s E_{\mu BI}$.

The displacement of the level-0 floor at the beginning and end of a half cycle is assumed as

$$y_0(t_1) = -\eta\delta_{GAP}, y_0(t_2) = \delta_{GAP}, \tag{8}$$

where η is the ratio of displacement and assumed to be $0 \le \eta \le 1$. The energy absorptions of the flexible and rigid-plastic elements, $\Delta_f E_{\mu BI}$ and $\Delta_s E_{\mu BI}$, are calculated as

$$\Delta_f E_{\mu BI} = \frac{1}{2}k_{0f}(1-\eta^2)\delta_{GAP}{}^2, \Delta_s E_{\mu BI} = {}_sQ_{0y}(1+\eta)\delta_{GAP}. \tag{9}$$

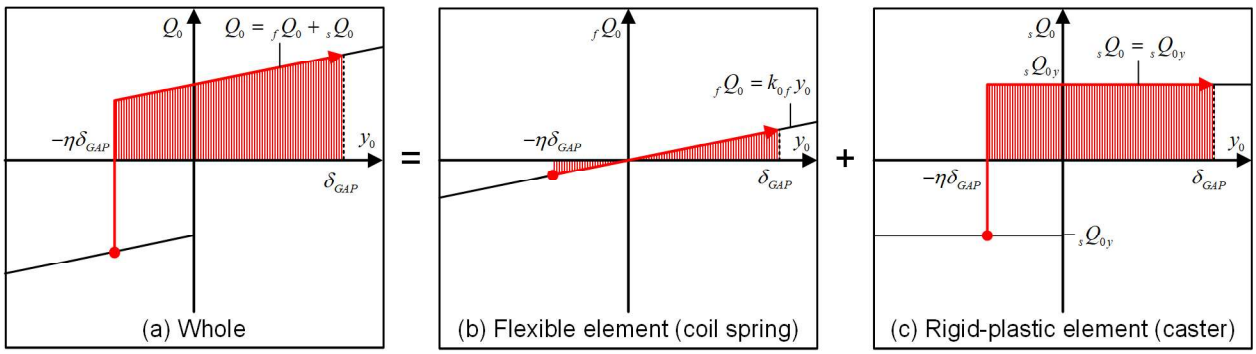

Figure – 11 Modeling of the capacity of energy absorption at the base-isolation layer

Taking the average of the expression in Eq. (9) with respect to η in the range $[0,1]$, the capacity of energy absorption at the base-isolation layer, $\Delta E_{\mu BI}$, is calculated as

$$\Delta E_{\mu BI} = \int_0^1 \left\{ \frac{1}{2}k_f(1-\eta^2)\delta_{GAP}{}^2 + {}_sQ_{0y}(1+\eta)\delta_{GAP} \right\} d\eta = \frac{1}{3}k_f\delta_{GAP}{}^2 + \frac{3}{2}{}_sQ_{0y}\delta_{GAP}. \tag{10}$$

5.2 Evaluation of properties of the base-isolation layer

As shown in Eq. (10), two parameters of the base-isolation layer, namely the horizontal stiffness of the coil springs k_{0f} and rolling friction force of the caster wheels ${}_sQ_{0y}$ are needed for the calculation of the capacity of energy absorption at the base-isolation layer. In this study, the value of k_{0f} is taken from a catalog as 112 N/m. Meanwhile, the value of ${}_sQ_{0y}$ is determined from non-collision test results. Figure 11 shows the results of a non-pounding test.

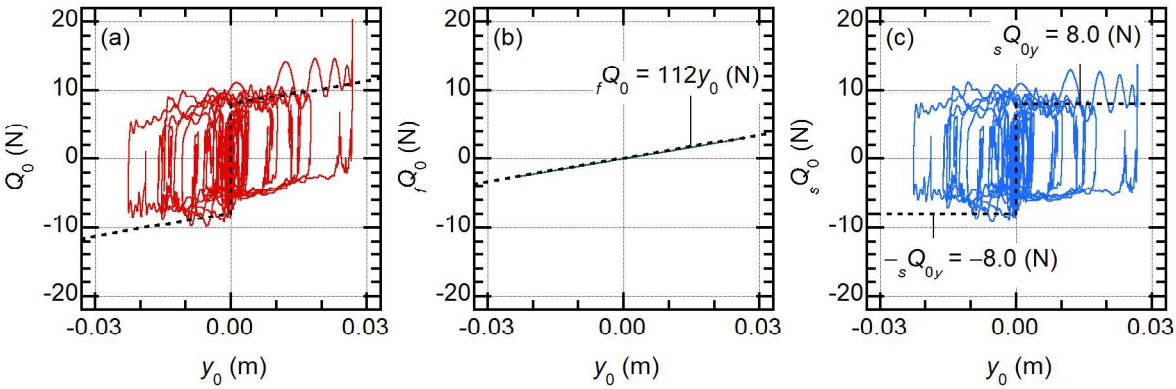

Figure – 12 Force–deformation relationship of the base-isolation layer obtained in a non-collision test (Model-1, ground motion: HAC, δ_{GAP} = 45 mm): (a) whole base-isolation layer, (b) flexible element, and (c) rigid-plastic element.

In Fig. 12, the shear forces of flexible and rigid-plastic elements, ${}_fQ_0(t)$ and ${}_sQ_0(t)$ respectively, are calculated as

$$ {}_fQ_0(t) = k_{0f} y_0,\ {}_sQ_0(t) = Q_0(t) - {}_fQ_0(t) = Q_0(t) - k_{0f} y_0 . \tag{11} $$

The rolling friction force of caster wheels ${}_sQ_{0y}$ is obtained from the results presented in Fig. 11(c) as 8.0 N. This corresponds to the rolling friction force calculated assuming that the rolling friction coefficient of a caster wheel is 0.08.

5.3 Criterion for the seismic pounding of a base-isolated building

Figure 13 shows the relation of the maximum resultant force above the isolation layer $Q_{0\max}$ and the ratio $\left(\Delta E_{\mu BI}/\Delta E_{\max}\right)$ obtained from the test results. In this figure, a red filled circle represents a collision case while a blue filled circle represents a non-collision case. All test results are divided into these two cases on the basis of a video recorded during the test and time history of the acceleration at level 0, $a_0(t)$; i.e., a case in which a sharp spike is observed in the acceleration response of level 0 shown in Fig. 3 is considered a "collision case". In this figure, most of the plots of collision cases are within the area $\left(\Delta E_{\mu BI}/\Delta E_{\max} < 1\right)$ while most of the plots of non-collision cases are within the area $\left(\Delta E_{\mu BI}/\Delta E_{\max} > 1\right)$. In addition, in all but one case, $Q_{0\max}$ is larger than 20 N when the ratio $\left(\Delta E_{\mu BI}/\Delta E_{\max}\right)$ is less than unity while $Q_{0\max}$ is smaller than 20 N when the ratio $\left(\Delta E_{\mu BI}/\Delta E_{\max}\right)$ is larger than unity.

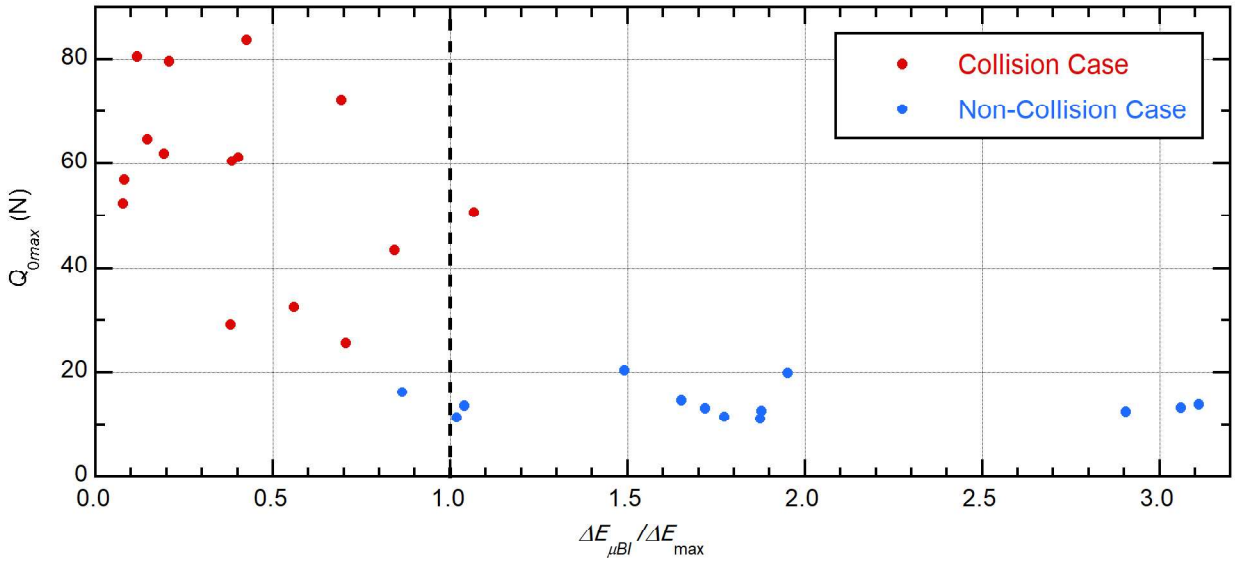

Figure – 13 Validation of the criterion of seismic pounding

In conclusion, the ratio $\left(\Delta E_{\mu BI}/\Delta E_{\max}\right)$ is a potential index with which to judge the possibility of seismic pounding. The ratio $\left(\Delta E_{\mu BI}/\Delta E_{\max}\right)$ should be larger than unity to avoid the seismic pounding.

6. Conclusion

The effect of the seismic pounding behavior of a base-isolated building on a retaining wall was experimentally investigated. A criterion for the seismic pounding of a base-isolated building was then discussed in terms of the maximum momentary energy input proposed by Hori and Inoue [8]. The main contribution and results of the paper are as follows.

(1) In the case of a flexible superstructure, the increase in acceleration due to pounding was limited to the lowest floor. However, in the case of a stiff superstructure, there was an increase in acceleration due to pounding on all floors. In addition, the fluctuation of the story shear force due to pounding was more remarkable when the superstructure was stiff. The story shear in the superstructure of the base-isolated model can be larger than that in the superstructure of the fixed-base model.

(2) The equivalent velocity of the maximum momentary input energy, calculated from the test results, is close to the elastic input energy spectra. The difference in the maximum momentary input energy due to the clearance size is negligible.

(3) The ratio of the capacity of energy absorption at the base-isolation layer, $\Delta E_{\mu BI}$, to the maximum momentary input energy, $\Delta E_{\max}$, is a potential index with which to judge the possibility of seismic pounding. The ratio $\left(\Delta E_{\mu BI}/\Delta E_{\max}\right)$ should be larger than unity to avoid seismic pounding.

Acknowledgement

We thank Takumi Ishida, Takumi Satoh and Yuga Shiraishi, for helping with the test and Glenn Pennycook, MSc, from Edanz Group (https://en-author-services.edanz.com/ac) for editing a draft of this manuscript.

References

[1] Architectural Institute of JAPAN (AIJ) (2016): *Design Recommendations for Seismically Isolated Buildings*. Architectural Institute of Japan.

[2] Architectural Institute of JAPAN (AIJ) (2007): *Structural Response and Performance for Long Period Seismic Ground Motion*. Architectural Institute of Japan. (In Japanese).

[3] Komodromos P (2008): Simulation of the earthquake-induced pounding of seismically isolated buildings. *Computers and Structures*, **86**, 618-626.

[4] Polycarpou PC, Komodromos P (2010): Simulating seismically isolated buildings under earthquake-induced pounding incidences. *Structures Under Shock and Impact XI, WIT Transactions on The Built Environment*, **113**, 245-256.

[5] Polycarpou PC, Komodromos P (2010): Earthquake-induced poundings of a seismically isolated building with adjacent structures. *Engineering Structures*, **32**, 1937-1951.

[6] Pant DR, Wijeyewickrema AC (2012): Structural performance of a base-isolated reinforced concrete building subjected to seismic pounding. *Earthquake Engineering & Structural Dynamics*, **41** (12), 1709-1716.

[7] Sasaki T, Sato E, Fukuyama K, Kajiwara K (2017): Enhancement of base-isolation based on E-Defense full-scale shake table experiments: dynamic response of base-isolated building under impact due to pounding. *16th World Conference on Earthquake Engineering 16WCEE*, Santiago Chile.

[8] Hori N, Inoue N (2012): Damaging properties of ground motion and prediction of maximum response of structures based on momentary energy input. *Earthquake Engineering & Structural Dynamics*, **31** (9), 1657-1679.

